第34卷 第3期 焊 接 学 报 Vol. 34 No. 3
2013年3月 TRANSACTIONS OF THE CHINA WELDING INSTITUTION March 2013

铝合金疲劳裂纹扩展声发射监测

朱荣华， 刚 铁
（哈尔滨工业大学 现代焊接生产技术国家重点实验室，哈尔滨 150001）

摘 要： 采用声发射（acoustic emission，AE）技术对7N01铝合金单边缺口三点弯曲试样不同应力比、不同峰值载荷下疲劳裂纹扩展过程中声发射信号进行了监测，建立了裂纹扩展速率、声发射计数（count）与应力强度因子之间的关系. 结果表明，大部分的声发射信号主要产生于疲劳循环载荷的低应力阶段，这主要是低应力阶段的声发射活动主要与裂纹尖端的塑性变形和裂纹闭合现象有关，声发射计数与应力强度因子之间呈指数增长的关系. 基于所建立的声发射计数率与裂纹扩展速率的关系，可以预测疲劳损伤结构的剩余寿命.

关键词： 铝合金； 声发射； 疲劳； 计数
中图分类号： TG146.21 **文献标识码：** A **文章编号：** 0253－360X(2013)03－0029－04


朱荣华

0 序 言

随着车辆轻量化的发展，铝合金结构在车体制造中得到越来越广泛的应用[1,2]. 车体的铝合金结构在服役过程中，受到循环载荷的作用，会在多个位置产生微裂纹，这些裂纹缓慢长大，汇集，最终形成沿平面最大拉应力的主裂纹，当主裂纹生长到一定尺寸时，导致铝合金结构的失效[3].

声发射技术与传统的无损检测方法相比具有连续监测的特点，可应用于结构的服役在线监测[4]. 采用声发射技术评估结构疲劳损伤，关键是建立疲劳裂纹参数与声发射信号特征之间的关系. 根据线弹性断裂机制，裂纹长度、裂纹扩展速率、应力强度因子区间等参数被用来评估结构的疲劳损伤. 许多学者尝试建立声发射参数与材料行为之间的关系[5－10]. Dunegan等人建立了声发射振铃计数与应力强度因子之间的关系：$\frac{\mathrm{d}\eta}{\mathrm{d}N}=B(\Delta K)^{p}$. GangQi建立了声发射小波能量与应力强度因子之间的关系.

文中基于声发射技术对7N01铝合金母材和焊缝疲劳裂纹扩展过程进行了监测，建立了裂纹扩展速率、声发射计数与应力强度因子之间的关系，为疲劳损伤预测奠定了基础.

收稿日期：2012－07－30
基金项目：国家自然科学基金资助项目（51175113）；国际合作基金（2007DFR70070）资助项目

1 公式推导

根据线弹性断裂理论，疲劳裂纹扩展速率可由Paris方程，得

$$\frac{\mathrm{d}a}{\mathrm{d}N}=C(\Delta K)^{m} \tag{1}$$

$$\lg\left(\frac{\mathrm{d}a}{\mathrm{d}N}\right)=\lg C+m\lg(\Delta K) \tag{2}$$

式中：a 为裂纹长度；N 为疲劳寿命；ΔK 为应力强度因子区间；C 和 m 为材料相关的常数. 声发射信号的特征参数如计数、能量等与裂纹长度及应力强度因子范围也存在如下关系[6]，即

$$\frac{\mathrm{d}\eta}{\mathrm{d}N}=B(\Delta K)^{p} \tag{3}$$

$$\lg\left(\frac{\mathrm{d}\eta}{\mathrm{d}N}\right)=\lg B+p\lg(\Delta K) \tag{4}$$

式中：η 为AE计数；B 和 p 为材料常数；对于标准SEB试样，应力强度因子区间的计算公式为

$$\Delta K=\frac{\Delta pS}{bW^{\frac{3}{2}}}*f(\alpha) \tag{5}$$

$$f(\alpha)=\frac{3(\alpha)^{\frac{1}{2}}[1.99-\alpha(1-\alpha)(2.15-3.93\alpha+2.7\alpha^{2})]}{2(1+2\alpha)(1-\alpha)^{\frac{3}{2}}} \tag{6}$$

式中：$\alpha=a/W$；b 为试样厚度；W 为试样宽度；S 为跨距；Δp 为载荷范围.

2 试验材料与设备

2.1 试验材料

试验材料为列车车体结构制造中广泛应用的 7N01 铝合金. 采用 TIG 焊焊接铝合金试板. 母材和焊缝的力学性能如表 1 所示. 根据 ASTM E647 标准制备了母材和焊缝的单边缺口三点弯曲试样,试样几何尺寸如图 1 所示.

表 1 7N01 铝合金母材和焊缝的力学性能

Table 1 Mechanical properties of 7N01 aluminum alloy base metal and weld

7N01 铝合金	抗拉强度 R_m/MPa	屈服强度 R_{eL}/MPa	弹性模量 E/GPa
母材	365	295	91.5
焊缝	274	210	82.4

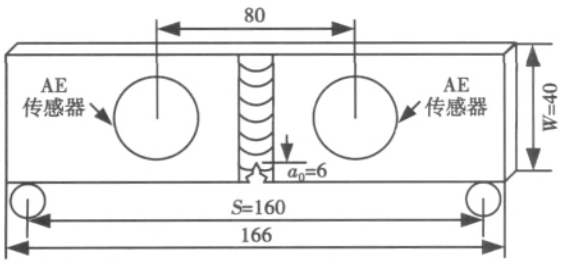

图 1 疲劳试样尺寸及形状(mm)

Fig. 1 Shape and size of fatigue specimens

2.2 试验设备及测试过程

疲劳裂纹扩展试验在 MTS809 伺服液压试验机上进行,疲劳试样的试验参数如表 2 所示. 所有试样的加载频率为 4 Hz,裂纹长度测量采用 COD 规定. 采用降 K 法预制 4 mm 的疲劳裂纹.

表 2 疲劳试验的载荷及应力比

Table 2 Load and stress ratio during fatigue tests

试样类型	试样编号	厚度 B/mm	宽度 W/mm	载荷区间 ΔP/kN	应力比 R
单边缺口	SEB1	12	40	0.8 ~ 8	0.1
母材试样	SEB2	12	40	2.4 ~ 8	0.3
单边缺口	SEB3	12	40	4 ~ 8	0.5
焊缝试样	SEB4	12	40	1 ~ 10	0.1
Welded SEB	WSEB1	12	40	0.8 ~ 8	0.1

使用 PCI-2 声发射采集系统监测疲劳裂纹扩展过程中的 AE 信号,两个谐振式 AE 传感器 R15I-AST 被对称放置在预制裂纹两侧,传感器与试样之间采用凡士林耦合,并用胶带固定(传感器位置如图 1 所示),传感器获取的信号通过前置放大器(增益为 40 dB)放大后,由计算机采集存储. 采样频率为 5 MHz.

3 试验结果

3.1 疲劳裂纹扩展速率特征

图 2 为 7N01 铝合金母材和焊缝在不同应力比和峰值载荷下的裂纹长度与疲劳寿命关系曲线. 从图 2 中可以看出,在低应力比和高峰值载荷下母材裂纹扩展速度较快.

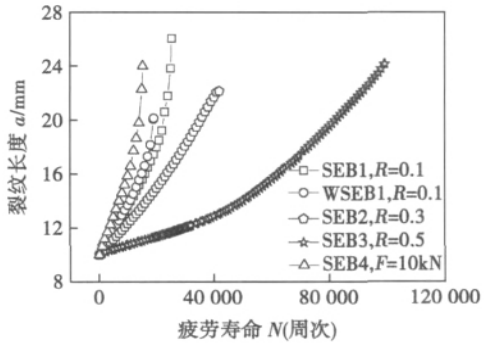

图 2 母材与焊缝裂纹长度与疲劳寿命关系

Fig. 2 Diagram of crack length versus fatigue cycles for base metal and weld

图 3 为 7N01 铝合金母材和焊缝在不同应力比和峰值载荷下的裂纹扩展速率与应力强度因子关系曲线. 从图 3 中可以看出,在不同应力比和峰值载荷下,母材和焊缝在疲劳裂纹扩展阶段遵循 Paris 法则. 在相同的 ΔK 下,母材裂纹扩展速率(da/dN)随着应力比的减小、峰值载荷的增加而增加.

3.2 疲劳裂纹扩展过程中的 AE

图 4 为 7N01 铝合金母材和焊缝在应力比为 0.1,峰值载荷为 8 kN 疲劳过程中声发射计数随疲劳载荷和循环周期变化的三维柱状图. 三维柱状图代表了疲劳循环过程中不同应力状态下声发射信号的活跃程度.

从图 4 中可以看出,疲劳裂纹稳定扩展阶段,大部分的声发射信号主要产生于循环载荷的低应力阶段,这主要是低应力阶段的声发射活动主要与裂纹尖端的塑性变形和裂纹闭合现象有关[11]. 随后,在疲劳裂纹扩展的第三个阶段,可以看出声发射信号的产生开始向高应力循环阶段转变.

3.3 声发射数据与裂纹扩展速率

采用七点递推多项式法计算了裂纹扩展速率,

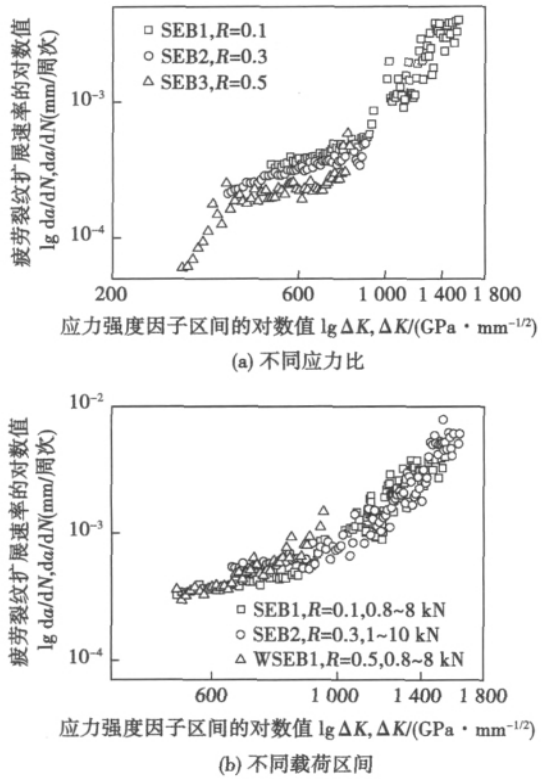

图 3　母材、焊缝裂纹扩展速率与应力强度因子区间关系

Fig. 3　Diagram of crack growth rates versus stress intensity factors range for base metal and weld

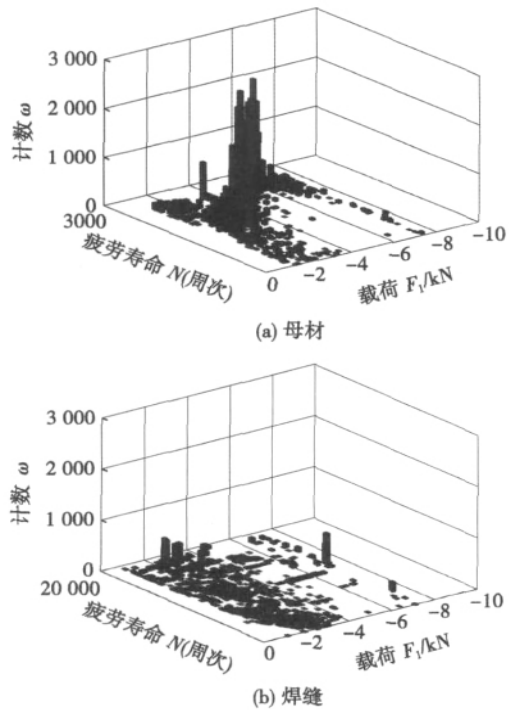

图 4　声发射计数随疲劳载荷和循环次数变化图

Fig. 4　Diagram of AE counts changes with fatigue load and cycles

并对裂纹扩展速率与应力强度因子区间进行了线性拟合，拟合数据如表 3 所示.

表 3　疲劳裂纹扩展速率与声发射计数率

Table 3　Crack growth rates and AE count rate

试样编号	初始裂纹 l_1/mm	疲劳寿命 N(周次)	裂纹扩展速率		声发射计数率	
			m	lg$C$	p	lg$B$
SEB1	9.990	25 378	0.79	−5.63	5.47	−15.41
SEB2	9.995	41 891	0.81	−5.76	7.27	−20.96
SEB3	10.004	99 319	0.68	−5.52	4.29	−12.77
SEB4	9.985	15 264	0.85	−5.69	3.40	−9.18
WSEB1	9.996	19 163	1.86	−8.60	1.36	−3.01

由式(2)，式(4)可以推导出计数率与裂纹扩展速率之间的关系为

$$\lg\left(\frac{\mathrm{d}a}{\mathrm{d}N}\right)=\frac{m}{p}\lg\left(\frac{\mathrm{d}\eta}{\mathrm{d}N}\right)+\lg\left(\frac{C}{B^{\frac{m}{p}}}\right) \tag{7}$$

基于试验数据，母材计数率与裂纹扩展速率之间的关系可表示为

$$\lg\left(\frac{\mathrm{d}a}{\mathrm{d}N}\right)=0.15\times\lg\left(\frac{\mathrm{d}\eta}{\mathrm{d}N}\right)-3.42 \tag{8}$$

采用相同的方法(七点递推多项式法)对声发射数据进行了统计分析(图 5)，声发射计数率与裂

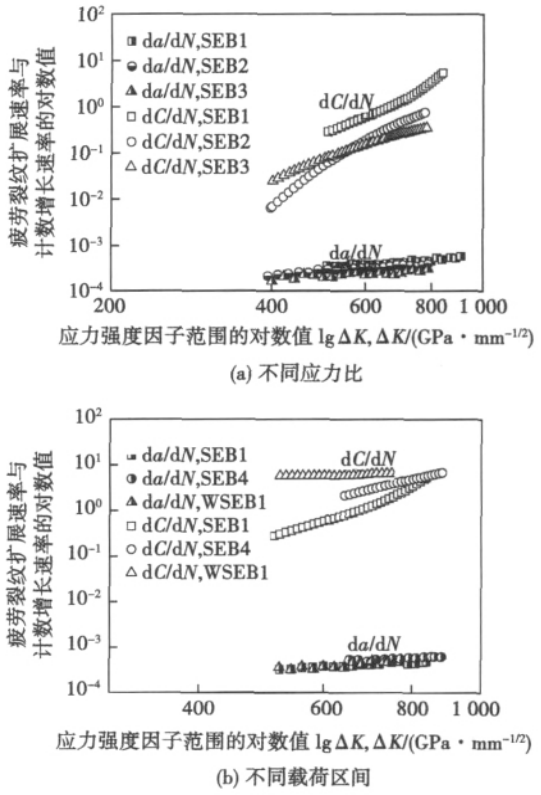

图 5　裂纹扩展速率、AE 计数率与应力强度因子区间关系

Fig. 5　Diagram of crack propagation and AE count rates versus stress intensity factor range for base metal and weld

纹扩展速率之间的关系为

$$\lg\left(\frac{\mathrm{d}a}{\mathrm{d}N}\right)=1.37\times\lg\left(\frac{\mathrm{d}\eta}{\mathrm{d}N}\right)-4.48 \qquad (9)$$

4 结 论

(1) 母材试样在低应力比和高的峰值载荷下，裂纹扩展速率较快. 焊缝与母材相比，具有较快的裂纹扩展速率.

(2) 疲劳裂纹稳定扩展阶段，大部分的声发射信号主要产生于循环载荷的低应力阶段，这主要是低应力阶段的声发射活动主要与裂纹尖端的塑性变形和裂纹闭合现象有关.

(3) 建立了母材和焊缝声发射计数率与裂纹扩展速率之间的关系，可为铝合金疲劳损伤的剩余寿命预测提供依据.

参考文献：

[1] 路 浩，马子奇，刘雪松，等. 300 km/h 高速列车车体残余应力超声波法无损测量 [J]. 焊接学报，2010，31(8)：29 - 33.
Lu Hao，Ma Ziqi，Liu Xuesong，*et al*. Ultrasonic residual stress measurement of 300 km/h high-speed train body [J]. Transactions of the China Welding Institution，2010，31(8)：29 - 33.

[2] 路 浩，刘雪松，孟立春，等. 高速列车车体服役状态残余应力超声波法无损测量及验证 [J]. 焊接学报，2010，31(8)：29 - 33.
Lu Hao，Liu Xuesong，Meng Lichan，*et al*. Residual stress evaluation of high-speed train body structure by ultrasonic method and verification [J]. Transactions of the China Welding Institution，2010，31(8)：29 - 33.

[3] 陆善平，魏世同，李殿中，等. 焊丝成分对高速列车转向架焊接接头性能的影响 [J]. 焊接学报，2010，31(6)：21 - 24.
Lu Sanping，Wei Shitong，Li Dian zhong，*et al*. Effects of welding wire composition on properties of welding joints for high-speed train bogie [J]. Transactions of the China Welding Institution，2010，31(6)：21 - 24.

[4] Joselin R，Chelladurai T. Burst pressure prediction of composite pressure chambers using acoustic emission technique：a review [J]. Journal of Failure Analysis and Prevention，2011，11：344 - 356.

[5] Ahmed Maslouhi. Fatigue crack growth monitoring in aluminum using acoustic emission and acousto-ultrasonic methods [J]. Structural Control and Health Monitoring，2011，18：790 - 806.

[6] Harris D O，Dunegan H L. Continuous monitoring of fatigue crack growth acoustic emission techniques [J]. Nondestructive Testing and Evaluation，1998，14：71 - 87.

[7] Morton T M，Harrington R M，Bjeletich J G. Acoustic emission of fatigue crack growth [J]. Engineering Fracture Mechanics，1973，5：691 - 697.

[8] Hamel F，Bailon J P，Bassim M N. Acoustic emission mechanisms during high-cycle fatigue [J]. Engineering Fracture Mechanics，1981，14：853 - 860.

[9] Sinclair A C E，Connors D C，Formby C F. Acoustic emission analysis during fatigue crack growth in steel [J]. Materials Science and Engineering，1977，8：263 - 273.

[10] 李光海，刘正义. 基于声发射技术的金属高频疲劳监测 [J]. 中国机械工程，2004，13：1205 - 1209.
Li Guanghai，Liu Zhengyi. Inspection of metal high frequency cyclic fatigue behavior utilizing acoustic emission technique [J]. China Mechanical Engineering，2004，13：1205 - 1209.

[11] Denial I M，Luo J J，Sifniotopoulos C G. Acoustic emission Monitoring of fatigue damage in metals [J]. International Journal of Plasticity，2003，19(6)：771 - 804.

作者简介： 朱荣华，男，1981 年出生，博士研究生. 主要从事声发射检测方面的科研. 发表论文 1 篇. Email：ronghua810@yahoo.cn

通讯作者： 刚 铁，男，博士，教授，博士生导师. Email：gangt@hit.edu.cn

[上接第 28 页]

(3) 切割完成后，如需要对工件进行进一步的精密加工，则应将火焰切割造成的热影响区部分用切削的方法去除从而得到组织性能理想的工件，需要去除的部分称为机械加工余量，机械加工余量应覆盖热影响区的部分.

参考文献：

[1] 梁桂芳. 切割技术手册 [M]. 北京：机械工业出版社，1997.

[2] DIN EN 10083 - 3 - 2006，Steel for quenching and tempering part 3 technical delivery conditions for alloy steels [S]，2006.

[3] 《中国航空材料手册》编辑委员会. 中国航空材料手册 [M]. 2 版. 北京：中国标准出版社，2001.

[4] 周振丰. 焊接冶金学 [M]. 北京：机械工业出版社，1995.

[5] 曹良裕，魏战江. 钢的碳当量公式及其在焊接中的应用 [J]. 材料开发与应用，1999，14(8)：39 - 43.
Cao Liangyu，Wei Zhanjiang. Formula of carbon equivalent and application in welding [J]. Development and Application of Materials，1999，14(8)：39 - 43.

作者简介： 韩永旭，男，1965 年出生，高级工程师. 主要从事热切割工艺与设备方面的研究. 发表论文 10 篇. Email：hwihyk@163.com

joint was excellent due to the slight interface migration, and fracture occurred in the top sheet. However, when the interfaces at both sides of weld moved downward, fracture occurred in the bottom sheet. The shear strength decreased with increase of the height of interface migration. The shear strength was higher when the load was exerted on the advancing side than on the retreating side.

Key words: friction stir welding; lap joint; plunge depth of shoulder; interface migration; mechanical properties

Effects of welding parameters on temperature field in GTAW ZHAO Ming, DU Dandan, LUO Detong (College of Mechanical and Electronic Engineering, China University of Petroleum, Qingdao 266580, China). pp 20 – 24

Abstract: Numerical analysis of heat transfer in gas tungsten arc welding (GTAW) process was conducted with ANSYS software. The calculated results of transient evolution of isotherms during continuous welding for 20 s and cooling for 20 s show that the workpiece was completely penetrated at 5 s after the arc was struck, however, the molten pool totally disappeared within 1 s after the arc moved away. During the welding process, the high-temperature region moved simultaneously with the arc. When the arc moved away, the cooling stage began, the zone with high temperature gradually moved backward (relative to the welding direction) and cooled to ambient temperature. The predicted thermal cycles at different points with the same intervals on top surface along the welding direction displayed that the temperature rising curves have the same trend in quasi-steady state, while clear differences existed between the temperature decreasing curves because the latent heat was released when the molten metal solidified. The temperature decreased faster at points closer to the weld crater. The influences of welding current, welding speed and concentration parameter on the heat transfer were analyzed, and then these parameters were optimized.

Key words: Gaussian heat source; distribution parameter of heat flux; gas tungsten arc welding; numerical analysis

Microstructure and mechanical properties in heat-affected zone of large-thickness steel ingot cut with oxygen-propane flame HAN Yongkui[1], WANG Zhixin[1], YAN Jiashu[1], LIN Yaowu[2], ZHAO Xianhong[2], MEI Longtian[2] (1. Harbin Welding Institute, China Academy of Machinery Science and Technology, Harbin 150080, China; 2. HengDing Shipbuilding Heavy Industry Co., Ltd., Suzhou 215513, China). pp 25 – 28, 32

Abstract: The machining allowance of precision metal cutting machine tools depends on the microstructure evolution in heat-affected zone during flame cutting. In this paper, 900 mm thick 34CrNiMo6 steel and 450 mm thick 45 carbon steel ingots were cut using an oxygen-propane flame. Then, the macroscopic morphology and microstructure in the heat-affected zone were examined to analyze the influence of microstructure evolution on the performance of workpieces. The range of heat-affected zone and machining allowance were determined to optimize the parameters during cutting and after cutting process.

Key words: flame cutting; large cross-section; steel; microstructure; heat-affected zone

Fatigue crack propagation of aluminum alloy based on acoustic emission monitoring ZHU Ronghua, GANG Tie (State Key Laboratory of Advanced Welding and Joining, Harbin Institute of Technology, Harbin 150001, China). pp 29 – 32

Abstract: The acoustic emission technique was used to monitor the fatigue crack propagation of 7N01 aluminum alloy single-edge notched three-point bend specimens under different stress ratio and peak load. The relationship between the crack growth rate, acoustic emission count rate and stress intensity factor range was established. The results show that most of the acoustic emission signals were produced in the low stress cyclic loading stage because the acoustic emission activity in low-stress phase was mainly related to the plastic deformation and crack closure in crack tip, and the acoustic emission count exponentially grew with the stress intensity factor. Based on the relationship between the acoustic emission count rate and crack growth rate, the remaining life of fatigue-damaged structures could be predicted.

Key words: aluminum alloy; acoustic emission; fatigue; counts

Arc pressure measurement and analysis of coupling arc AA-TIG HUANG Yong[1,2], QU Huaiyu[1], FAN Ding[1,2], LIU Ruilin[1], KANG Zaixiang[1], WANG Xinxin[1] (1. State Key Laboratory of Gansu Advanced Non-ferrous Metal Materials, Lanzhou University of Technology, Lanzhou 730050, China; 2. Key Laboratory of Non-ferrous Metal Alloys, The Ministry of Education, Lanzhou University of Technology, Lanzhou 730050, China). pp 33 – 36

Abstract: In order to study the coupling arc AA-TIG (arc assisted activating tungsten inert gas) welding, a static keyhole method was used to measure the arc pressure with stainless steel as the anode. The influence of main process parameters on the distribution of arc pressure was analyzed. Compared to the conventional TIG welding process under the same conditions, the peak value of arc pressure during the coupling arc AA-TIG welding was significantly reduced. With the welding current decreasing, the electrode distance increasing, the arc length increasing and the oxygen content of the assisted arc decreasing, the peak value of arc pressure in coupling AA-TIG welding decreased. The distribution of arc pressure was in concordance with Gaussian distribution at 2 mm electrode distance. With the electrode distance increasing, the distribution gradually turned into bimodal distribution.

Key words: AA-TIG; coupling arc; oxygen element; arc pressure; high-speed welding

Influence of weld shaping with trailing impact rolling on hardness and residual stress of under-matched equal load-carrying joint YANG Jianguo[1], WANG Jiajie[2], DONG Zhibo[2], FANG Hong yuan[2], ZHOU Lipeng[3] (1. Institute of Process Equipment and Control Engineering, Zhejiang University of Technology, Hangzhou 310014, China; 2. State Key Laboratory of Advanced Welding and Joining, Harbin Institute of Technology, Harbin 150001, China; 3. CGNPC Inspection Technology Co. Ltd, Suzhou 215004, China). pp 37 – 40